

# Data Acquisition System and Experimental Set-up for Wind Tunnel Study of 304CZ Sailplane's Winglets

Ing. P. Anderle  
*Aerospace Engineering Department  
Technical University in Prague  
Czech Republic*

Dr. L. Smrcek, Prof. F. Coton  
*Aerospace Engineering Department  
University of Glasgow  
Scotland, UK*

XXVII OSTIV Congress, Leszno, Poland, 2003

## Abstract

This paper describes an experimental set-up and aerodynamic investigation of winglets developed for the 304 CZ Sailplane (Fig. 1), part of a study into the velocity and vorticity distributions in the flow field behind winglets, using hot-wire anemometry. In this study, effort was focused on gaining a greater understanding of what happens in the region where the winglet joins the wing. The measurements were performed in the Handley-Page wind tunnel, of the Department of Aerospace Engineering at the University of Glasgow. In order to carry out measurements with the hot-wire anemometry system, a new traverse mechanism was designed and manufactured. This traverse mechanism was integrated with the other test instrumentation and to create a complete measurement chain. The complete system allows fully automated hot wire measurements to be made over a defined area using programmable test parameters.

## Notation

|            |                                 |
|------------|---------------------------------|
| $\omega_x$ | Vorticity component in YZ plane |
| $b$        | Wing span                       |
| $Y, Z$     | Cross-stream coordinates        |
| $U_\infty$ | Free stream velocity            |
| $X$        | downstream distance             |

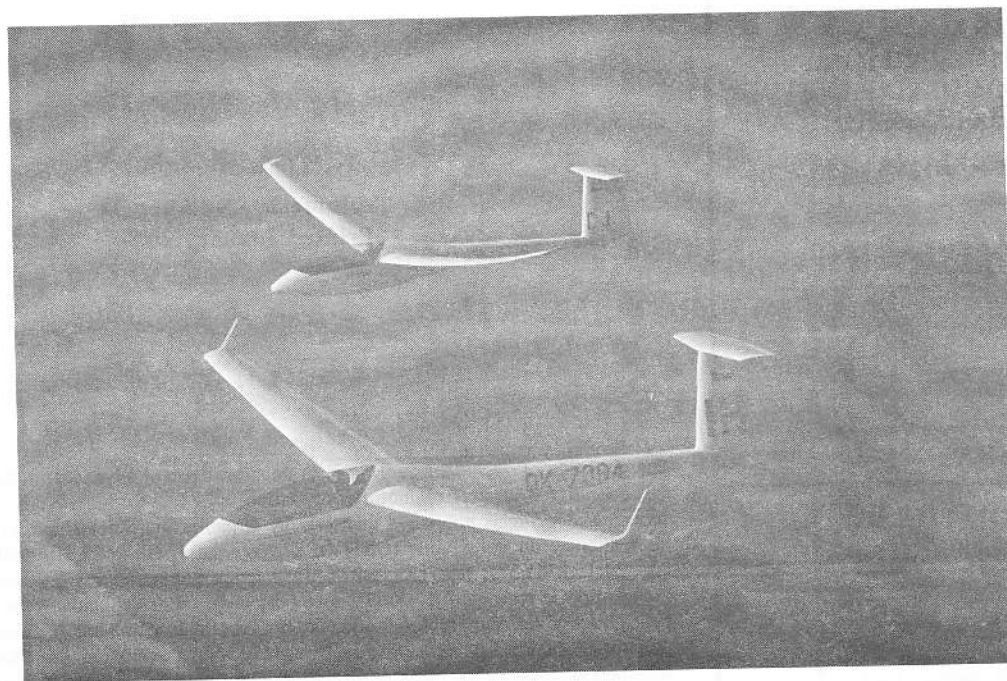


Figure 1. 304 CZ Sailplanes (photo by Jochen Ewald)

## Introduction

In the late 1960s, designers began experimenting with wing-tip geometries using 'small' vertical extensions to reduce the formation of tip vortices. The winglet concept actually dates back to 1897, when Frederick Lanchester took out a patent on the idea, incorporating it into some of his wing theories<sup>[1]</sup>. His wing had two 'capping planes' at the end of it, that became known in the 1920s as 'end plates', when Prandtl extended his basic lifting line concept<sup>[2]</sup>.

The real break-through with winglets was made by Whitcomb. In 1976, Richard Whitcomb, a NASA aerodynamicist, published a paper that compared a wing with a winglet and the same wing with a simple extension to increase its span<sup>[3]</sup>. Whitcomb showed that winglets reduced drag by about 20 percent and increased the wing lift-drag ratio by approximately 9 percent. Induced drag represents 30-40 percent of the total drag of a transport plane at the cruise condition, so the induced drag reduction has a significant effect on fuel consumption. Whitcomb began a focused investigation into winglet aerodynamics and tested several designs in the wind tunnels at NASA Langley Research Center. The first industry application of the winglet concept was in general aviation business jets. For instance, it is claimed that a winglet on a Boeing-747 could significantly reduce fuel burn on long-range flights. Research into the effect of winglets on first generation jet transport wings showed that they can produce reasonable drag reduction at high lift conditions<sup>[4]</sup>.

Winglets are now being incorporated into most new commercial and military transport jets. Since the 1980s, the most modern high performance sailplanes also have small vertical wing tip extensions.

The first sailplanes to have winglets were the ASW-19, GEMINI and NIMBUS 3. Sets of Whitcomb style winglets were fitted to these wings in the late 1980s. Flight tests carried out on these aircraft demonstrated the effect of winglets on high aspect ratio wings<sup>[5]</sup>.

### How Do Winglets Work

The primary effect of the winglet is to control the cross flow in the tip region of the wing in such a way as to reduce induced drag by displacing the vortices outward. The air flowing over the winglet, due to the presence of the tip vortex, strikes the winglet at an angle of attack. The winglet like any wing produces lift which, in this case, has a component in the forward direction. Thus, the winglet produces thrust (Fig. 2). This thrust component alters the cross flow at the wing tip and recovers some of the performance that would be lost through the additional drag caused by the increase in wetted area.

### Winglets For Sailplanes

Theory and experience has shown that the most efficient sailplane wing is one that is very long and slender. Having a high aspect ratio wing is one way of cutting wing-tip losses. In essence, the longer wing has the same tip losses but those

energy losses will affect a lesser proportion of the total wing. In other words, the lift is distributed over the longer wingspan and the trailing vorticity is spread out, dissipating less energy.

From a structural point of view, a long wing is prone to flex and has to be strengthened; this adds weight. The winglet provides the effect of an increased aspect ratio without extending the wing-span and so does not increase the wing root bending as much as an actual span extension would. The moment arm of the lift from a span extension is approximately one-half of the wing semi-span whereas the moment arm of the winglet lift is roughly only one-half of the vertical winglet span. This small increase does not overload the wing or significantly alter the standard operating limitations. The addition of winglets on sailplane wings also improves the maximum lift/drag ratio, which is of importance for sailplanes under span-limited FAI requirements<sup>[6]</sup>.

The induced drag coefficient is proportional to the square of the lift coefficient hence the reduction in drag also improves climbing capability<sup>[7][8]</sup>. This improvement can be used when sailplanes circle in thermal bubbles, the main source of energy to stay aloft<sup>[9]</sup>. To have a maximum cross country speed during sailplane competitions is another important consideration. Hence, the design of winglets must involve the compromise of maximizing the low speed improvement without sacrificing high-speed performance<sup>[10]</sup>.

The winglet added to an ASW-19 clearly showed that for some speeds the friction drag could exceed the induced drag reduction provided by winglets<sup>[11]</sup>. A correctly designed winglet can, however, be reasonably effective as illustrated in a study using the ASW-20 sailplane<sup>[12]</sup>.

### Wind Tunnel Models of Winglets

The wind tunnel models used in the experiments were real wing tips taken from the single seat, HpH 304CZ/C sailplane's wings.

The models were mounted vertically on a base plate that was secured to a rail track mechanism. This mechanism allowed the model to be moved backwards and forwards in the wind tunnel working section to change the distance between the model and the hot-wire measurement plane. In addition, the base plate was designed to allow the incidence of the model to be changed. During the experimental programme four kinds of wing tip were investigated; a wing without a winglet and then three 304CZ sailplane wing tips of different design. The key parameters that defined the winglet designs are shown in Fig. 3 and are the winglet airfoil, sweepback, cant angle, twist distribution and ratio of winglet root chord to winglet tip chord (taper).

### Wind Tunnel

The Handley Page wind tunnel is an atmospheric low-speed wind tunnel with a closed return circuit equipped with a rectangular testing-section of dimensions 2.15 m by 1.6 m and length 3.38 m (Fig. 4). The corners have 650 mm fillets that house lamps to provide lighting. Visual access to the working section is provided by 0,84 square meters of plate glass and

acrylic windows that permit the model to be viewed from many angles. Several venting slots in the tunnel walls at the test section exit maintain near atmospheric static pressure. The nozzle placed in front of testing section has a contraction ratio of 1:4. The power supply is an electric motor that drives a fan 2.3 m in diameter to provide the airflow in the wind tunnel. The tunnel can reach speeds up to 60m/s.

### Measurement Procedure

The measurement chain consists of x-wire sensor, a TSI IFA 300 constant temperature anemometry system, a personal computer, a SMOCI transmitter and a traversing mechanism as shown in Fig. 5. This figure also shows the model mounting arrangement described previously. The X-wire sensor is connected to two channels of the IFA 300 by coaxial cables. The IFA 300 hardware converts the acquired signals from the sensors and transmits them to the controlling computer via a BNC adapter block and data acquisition card. The IFA 300 software installed on computer then processes the recorded data. Once the data have been recorded for an entire X traverse, a master program, written in LABView, sends a new instruction to the SMOCI unit. The SMOCI converts the instruction into the signal needed by the stepper motors to move the traverse to its next Y position. When the traverse mechanism reaches this new position, another signal is sent to it and it begins its X traverse. The x-wire sensor continually samples data during this traverse and sends the signal to the computer. This process continues until measurements have been made over the entire measurement grid.

### Traverse Mechanism

The computer controlled traverse mechanism for probe positioning and data acquisition was specifically designed and manufactured for the present project. The traverse is a motorized two-component mechanism that can move the probe to any point within a 850mm x 930mm grid. In the present series of tests the traverse was mounted behind the test models such that measurements could be made in planes perpendicular to the onset flow. The location of the measurement plane with respect to the test model could be varied using the model mounting tracks described previously. The way in which the traverse is assembled is shown in Fig. 6 below and Fig. 7 shows the assembled traverse in the wind tunnel together with a winglet model.

The horizontal motion is provided by a large, off-the-shelf linear slide driven by a stepper motor. Vertical movement is provided by a purpose built traverse mechanism based on a precision ball screw which is positioned in front of a linear slide mounted on an aluminium box-section support. The carriage of the ball screw is connected to the carriage of the linear slide and so, when the ball screw is driven by a stepper motor, the carriage moves up and down. The incremental resolution of the linear motion is 0.03 mm.

### Hot Wire Anemometry

Measurements of the magnitude and associated direction of the time-dependent velocities behind the winglet models were obtained using a DANTEC 55P61 cross-wire probe connected to a TSI IFA-300 three-channel constant temperature

anemometer system. The sensor wires on the probe are 0.005mm diameter platinum plated tungsten wires with a length/diameter ratio of 250, which form a measuring volume of approximately 0.8mm in diameter and 0.5mm in height. The wires are orientated perpendicular to each other corresponding to 45 degrees from the free stream direction which gives the best angular resolution. An additional temperature probe was used to correct the anemometer output voltages for any variation in ambient flow temperature. For probe calibration, an open jet vertical wind tunnel with a maximum operating velocity of 43 m/s was used. A support allowed the sensors of the X-wire probe to be rotated by 30 degs in the plane of the sensors. Variation of the flow velocity and yaw angle then enabled the coefficients of the effective velocity method to be determined. Fig. 8 shows how the hot-wire anemometry system was integrated into the overall measurement system

### Investigation Grid

#### *Y-travel:*

One step of the stepper motor provides 0.03125 mm of linear motion and the time required for each step is 0.2980 seconds. The size of the investigation grid in the y-direction was 850 mm (Fig. 8) or 27200 steps of the stepper motor. The time required to traverse this distance was, therefore, 8.1055 sec.

At a sampling rate of 2000 Hz, the sampling time of 8.1055 seconds gives a total of 16211 investigation points per line. To allow for turbulence in the flow, the data are averaged in blocks of 48 measurement points corresponding to approximately 2.5mm of motion. Thus, 339 averaged data values are collected during each Y traverse.

#### *Z-travel*

The length of the investigation grid in the Z-direction was set at 600 mm. This length was divided into steps of 5 mm giving a total of 121 measurement points in the Z direction.

The total time taken to traverse the entire 850 mm x 600 mm grid was just over 20 minutes and a total of 41019 measurements were obtained for each grid. A schematic of this process is presented in Fig. 9.

### Experimental Results

The flow field behind the wing tip models was measured in three planes ( $X/b = 0.2$ ,  $X/b = 1$ ,  $X/b = 2$ ) for angles of attack  $\alpha = (-3, 0, 3, 6, 9)$  degree. For all tests the free stream velocity  $U_\infty$  was set at 33 m/s (118.8 Km/h) which corresponded to a Reynolds number of  $Re = 0.8 \times 10^6$  based on the mean chord of the main wing. Data analysis and graphical presentation were carried out using Tecplot software in the form of vector plots of velocity distribution and contour line plots of the vorticity component  $\omega_x$  defined in equation 1 and Fig. 10.

Figs. 11-14 present example measured data for four wing tip configurations in the plane  $X/b = 1$  when the wing was at an angle of attack  $\alpha = 3$  degrees and the free stream velocity was  $U_\infty = 33$  m/s. These figures illustrate the effectiveness of the system in capturing the differences in the flow structures

behind the different winglet configurations. For example, wing tip A (Fig. 11), which is basically a standard wing tip with a small vertical extension that projects downwards from the lower surface of the wing, produces an almost classical tip vortex structure where the vorticity is concentrated in a single structure that rolls up slightly inboard of the wing tip. Also visible in this figure is the vorticity in the wake of the main wing. Fig. 12, on the other hand, shows the velocity and vorticity distributions behind a much larger winglet extension. In this case, there are two clear vortex structures; one at the winglet/wing junction and the other at the tip of the winglet. The effect of sweeping this type of winglet back can be observed in Fig. 13, where measurements on a similar winglet with higher sweepback are presented. In this figure, the vorticity associated with the winglet/wing junction does not appear as a single well defined vortex but rather as a more spread-out region of vorticity. The winglet tip vortex is also less distinct but it should be remembered that the tip of the winglet will be closer to the measurement plane in this case and so the roll-up may not be as complete. Finally, the effect of a small upward swept winglet is shown in Fig. 14. In this case, the vorticity is well distributed and follows the curvature of the winglet. It should be noted that these cases are presented merely as an example of the capability of the measuring system. The evolution of the vortex structures downstream of these wing tips is very complex and cannot be inferred from observation of the behaviour at one measurement section alone.

### Conclusion

The experimental instrumentation for investigation of the flow field behind a winglet model has been designed, manufactured and set-up. A newly designed traverse mechanism has made it possible for measurements to be made at high spatial resolution within a large enough area for full size wing tip models to be tested. Results have been presented to demonstrate this capability. An additional feature of the system is that the time required for testing is also relatively short.

### Acknowledgement

The authors wish to acknowledge the support of the academic and technical staff of the University of Glasgow, Aerospace Engineering Department. Special thanks go to the technical staff from the Spencer Street Laboratory especially to Mr. R. Gilmour who helped with the experimental set-up and to Mr. T. Smedley, Mr. A. Erwin, Mr. J. Kitching and Mr. A. Fraser for their help in manufacturing and installing the equipment.

Special thanks should go to Mr J. Potmesil from HPH Ltd, Czech Republic, for his support in providing us with winglet models.

Mr P. Anderle was supported by a studentship provided by BAE Systems.

### References

- [1] Lanchester, F.W.: *Aerodynamics*, Constable & Co, London, 1907
- [2] Prandtl, L.: *Theory of lifting Surfaces*, *NACA TN9*, 1920
- [3] Whitcomb, R.T.: *A Design Approach and Selected Wind-Tunnel Result at High Subsonic Speed for Wing-Tip Mounted Winglets*, *NASA TN D-8260*, July 1976
- [4] Montoya, L.C., Jacobs, P.F., Flechner, S.G.: *Effect of Winglets on a First-Generation Jet Transport Wing, III-Pressure and Spanwise Load Distributions for a Semispan Model at Mach 0.3*, *NASA TN D-8478*, June 1977
- [5] Marsden, D.J.: *Winglets for Sailplanes*, *Technical Soaring*, Volume 15, No. 4, October 1991
- [6] Thorsen, O.R.: *Theoretical and Experimental Analysis of the Winglets designed for the High-Performance Sailplane ASW-27*, Thesis, TU Delft, March 1999
- [7] Nicks, O.W.: *Wing Extension for Improving Climb Performance*, *AIAA-83-2556*, October 1983
- [8] Nicks, O.W.: *A Physical View of Wing Aerodynamics*, *Technical Soaring*, Volume 17, No. 4, October 1993
- [9] Kiceniuk, T.: *Dynamic Soaring and Sailplane Energetic*, free flight-vol libre, Dec/Jan 2001
- [10] Smith, S.: *Do Winglets Work*, free flight-vol libre, Aug/Sep 1997
- [11] Masak, P.: *Winglet Design for Sailplanes*, free flight-vol libre, April/May 1992
- [12] Crosby, C.P., Ashman, P., Terblanche, H.: *Full-Scale In-Flight Pressure Measurements on a Winglet Fitted to an AS-W 20*, *Technical Soaring*, Volume 20, No. 3, July 1996

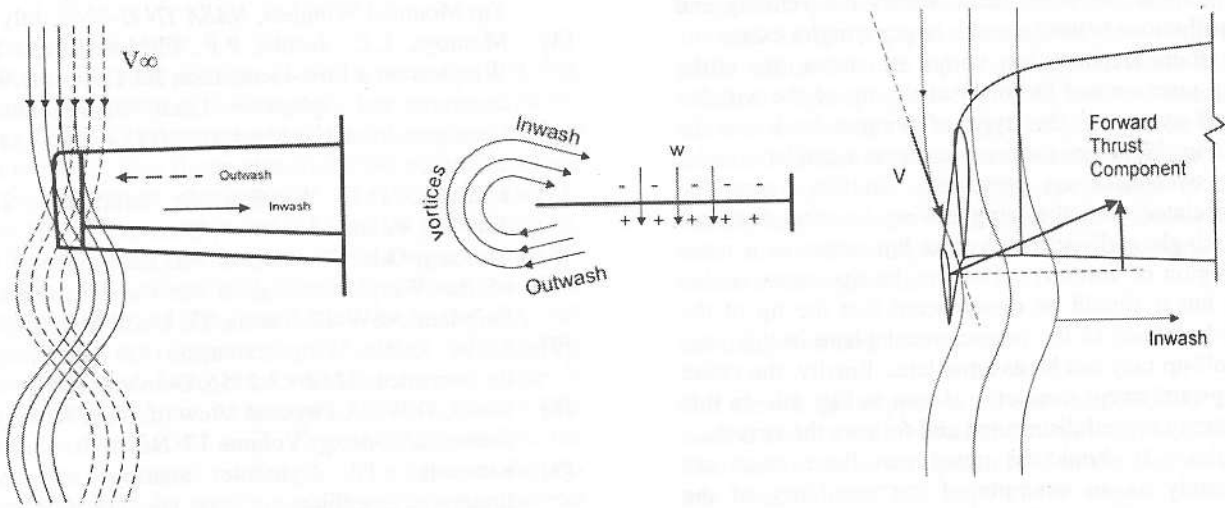


Figure 2. Forward Thrust Component Development

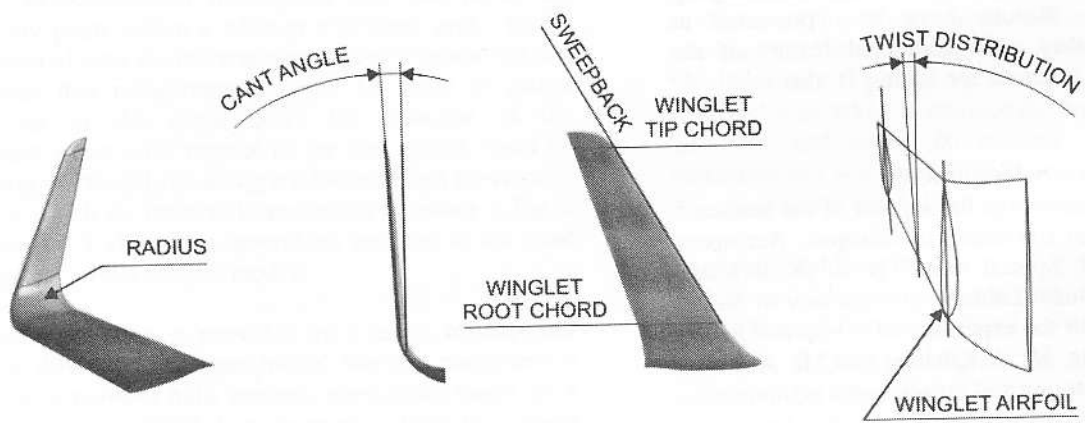


Figure 3. Key Parameters of Winglets

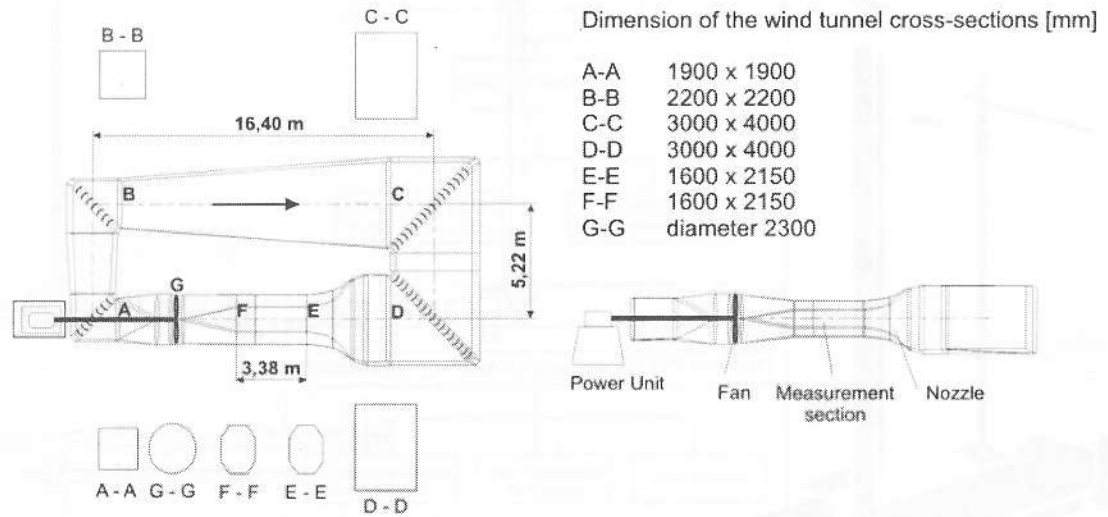


Figure 4. Handley Page Wind Tunnel, University of Glasgow

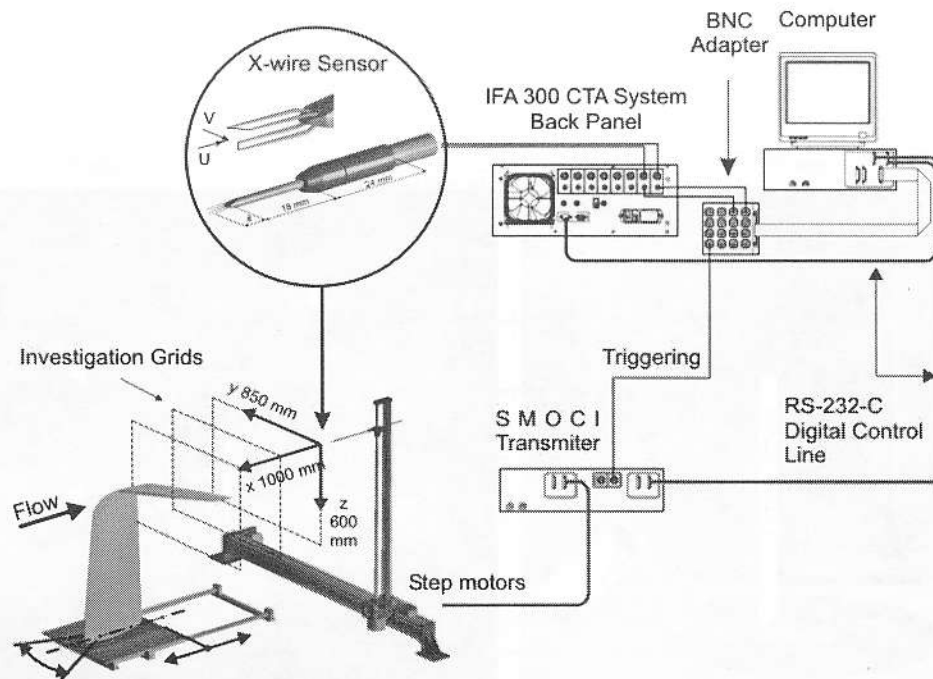
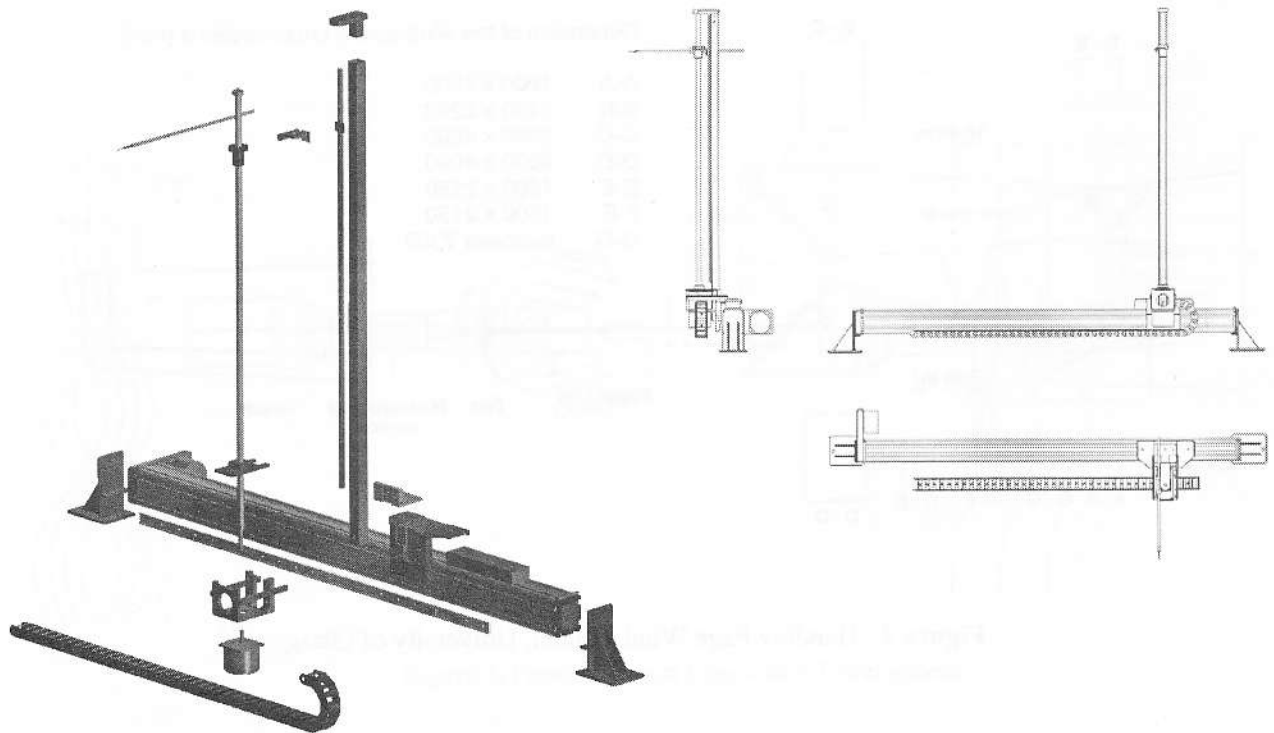
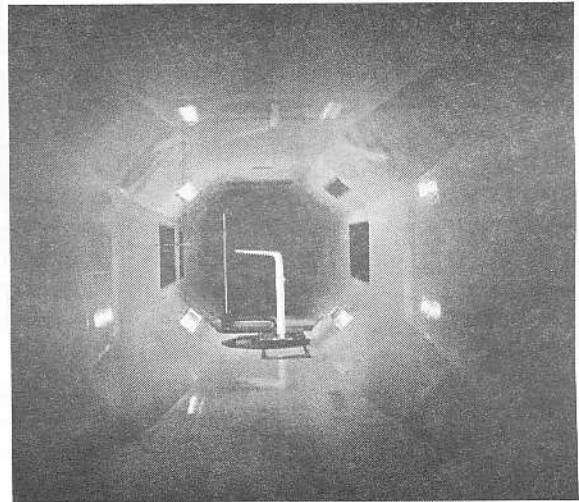
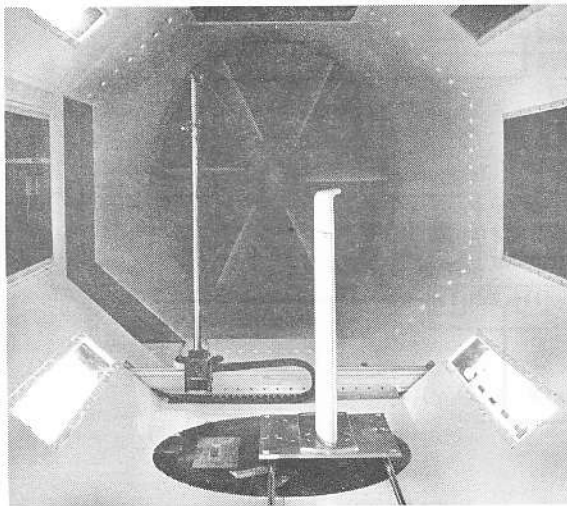


Figure 5. Wind Tunnel Testing Configuration



**Figure 6.** Traverse Mechanism



**Figure 7.** Winglet Models (1:1) Placed in Handley Page Wind Tunnel

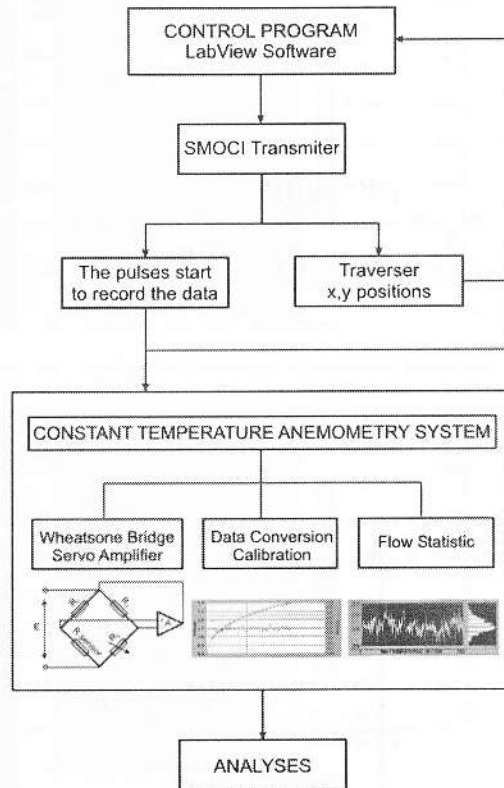


Figure 8. Flow Chart of Data Acquisition

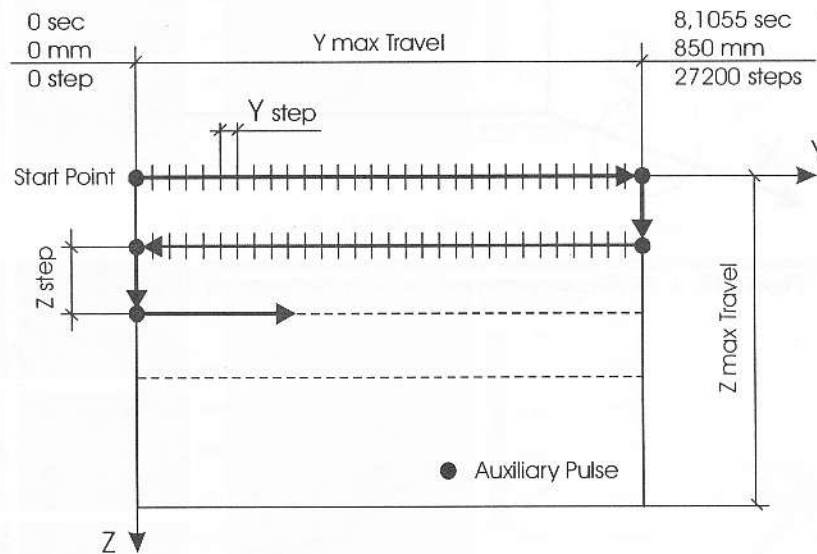
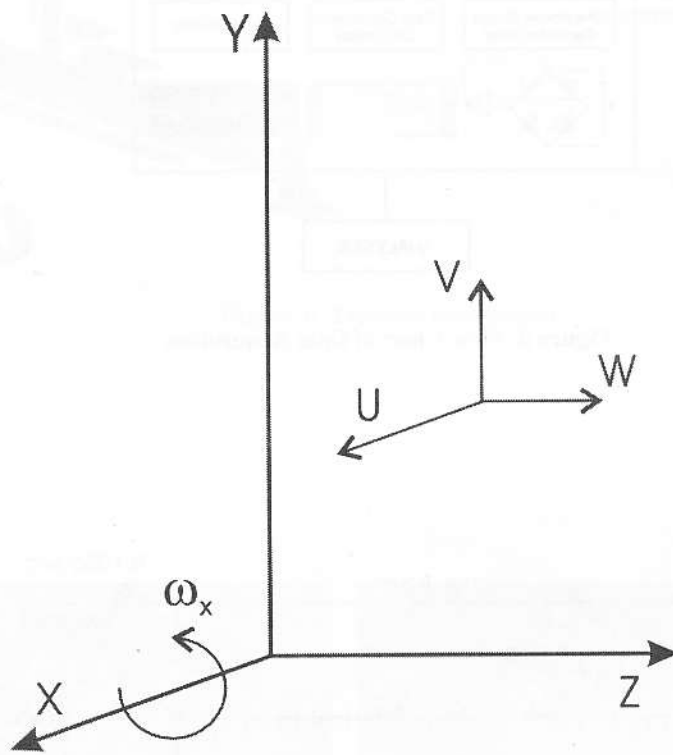


Figure 9. Investigation Grid

$$\omega_x = \frac{\partial V}{\partial z} - \frac{\partial W}{\partial y} \quad (1)$$



**Figure 10.** Coordinate system and velocity components definition

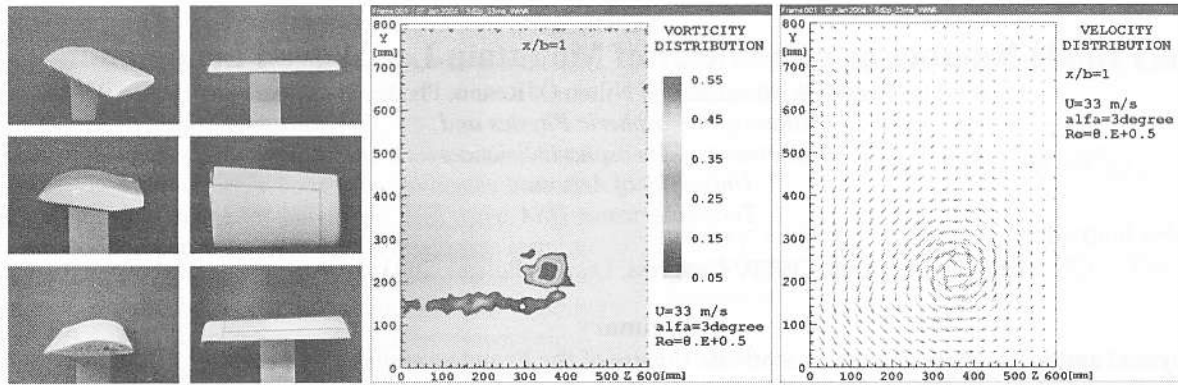


Figure 11. HpH 304 sailplane's standard wing tip - model A

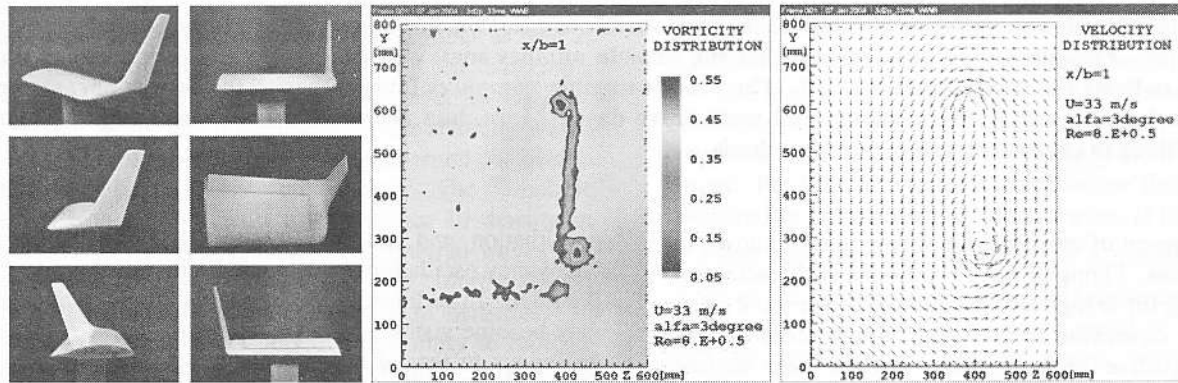


Figure 12. HpH 304 sailplane's detachable winglet - model B

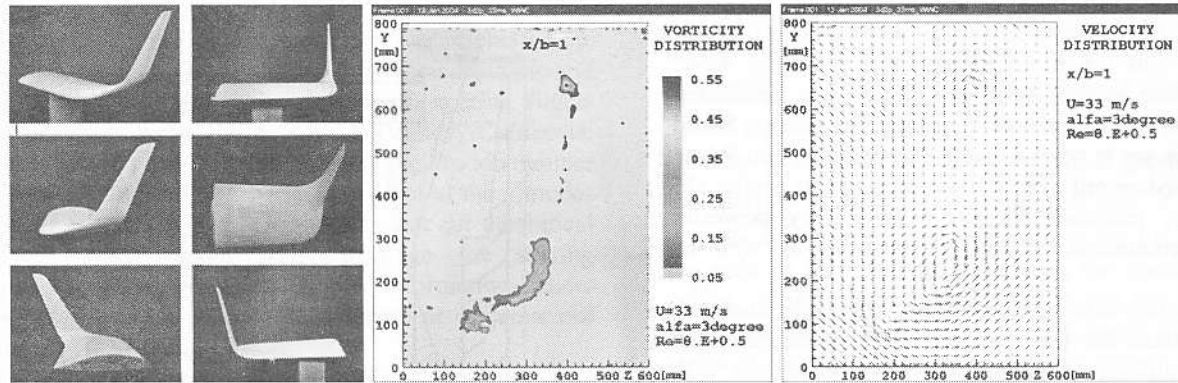


Figure 13. HpH 304 sailplane's winglet - model C

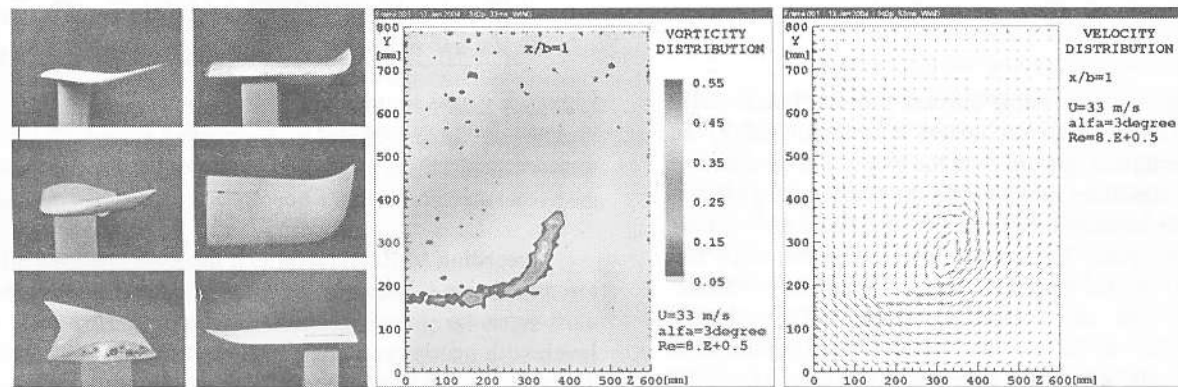


Figure 14. HpH 304 sailplane's wing tip for span of 17.43 meter - model D